Lattice Boltzmann Simulation of Reactive Microflows over Catalytic Surfaces

S. Succi, [1,2] **G. Smith,** [3] **and E. Kaxiras** [3]

We investigate the effects of geometrical micro-irregularities on the conversion efficiency of reactive flows in narrow channels of millimetric size with heterogeneous catalysis. Three-dimensional simulations, based upon a Lattice-Boltzmann-Lax–Wendroff code, indicate that micro-corrugations may have an appreciable effect on the effective reaction efficiency of the device. Once extrapolated to macroscopic scales, these effects can result in a sizeable increase of the overall reaction efficiency.

1. INTRODUCTION

Modern modelling science is confronted with phenomena of increasing complexity involving the simultaneous interaction of multiple spatio-temporal scales. The quantitative description of such complex phenomena commands sophisticated multidisciplinary approaches.[1] A typical example of such complex multiscale phenomena is the dynamics of reactive flows, a subject of wide interdisciplinary concern, with several applications in macro and micro-engineering, material science, biology, environmental and life sciences alike. The complexity of reactive flow dynamics is parametrized by three dimensionless quantities: the *Reynolds number* Re, the *Damkohler number* Da, and the *Péclet number* Pe. High Reynolds numbers are associated with turbulence, namely loss of coherence of the flow field in both

---

[1] Istituto di Applicazioni Calcolo, CNR, viale Policlinico 137, 00161 Roma, Italy; e-mail: succi@iac.rm.cnr.it

[2] Visiting Scholar, Lyman Laboratory of Physics, Harvard University.

[3] Lyman Laboratory of Physics, Harvard University, Cambridge, Massachusetts 02138.

space and time. High Damkohler numbers imply that chemistry is much faster than hydrodynamics, so that reactions are always in chemical equilibrium and take place in tiny regions (thin flames, reaction pockets) of evolving flow configurations. The opposite regime ("well-stirred" reactor) characterizes situations where the chemistry is slow and always takes place at local mechanical equilibrium. The Péclet number, defined as

$$\text{Pe} = \frac{UH}{D}$$

where U is a typical macroscopic flow speed, H a typical macroscopic length and D is the mass diffusivity of the generic transported species, plays a prominent role. High Péclet numbers imply that the transported species stick tightly to the fluid carrier (in the limit $\text{Pe} \to \infty$ the tracer field is "frozen-in" within flow streamlines). Conversely, low-Péclet regimes imply fast diffusion of the tracer across the flow field, efficient mixing hence higher reaction efficiency.

Navigation across the three dimensional Re–Da–Pe parameter space meets with an enormous variety of chemico-physical behaviours, ranging from turbulent combustion to hydrodynamic dispersion and many others.[2] The picture gets further complicated when geometry is taken into account, since boundary conditions select the spatio-temporal structures sustaining the non-linear interaction between the various fields. In this work we shall deal with *moderate-Reynolds, reacting flows with heterogeneus catalysis*. In particular, we wish to gain insight into the role of geometric micro-irregularities on the effective rate of absorption of tracer species (pollutant hereafter) at catalytic boundaries.

Given the fact that *almost all chemical reactions of industrial and biological relevance are catalytic*, the subject of catalytic absorption is a a theme of broad interest, with applications in biology, physics, chemistry and environmental sciences.[3]

This paper is organized as follows: In Section 2 we present the basic aspects of the mathematical model, while in Section 3 details of the computational model are discussed. In Section 4 we present some analytical considerations to estimate the effects of geometric irregularities on the catalytic efficiency. In Section 5 we present numerical results referring to a fast-reacting micro-channel flow with a single perpendicular barrier on the bottom wall. In Section 6 results pertaining to a slow-reacting flow with a trapezoidal corrugation are presented and compared with previous numerical and experimental data. Finally, some considerations on the need to assist numerical simulations with scaling theories to predict the efficiency of macroscopic devices are offered.

2. MATHEMATICAL MODEL OF REACTIVE MICROFLOW DYNAMICS

We shall deal with a *quasi-incompressible, isothermal flow* with soluted species which are transported (advect and diffuse) by the flow and, upon reaching solid walls, undergo *catalytic chemical reactions*. The basic equations of fluid motion are:

$$\partial_t \rho + \text{div } \rho \vec{u} = 0 \tag{1}$$

$$\partial_t \rho \vec{u} + \text{div } \rho \vec{u}\vec{u} = -\nabla P + \text{div}[\mu(\nabla \vec{u} + (\nabla \vec{u}))^T + \lambda \text{ div } \vec{u}] \tag{2}$$

where ρ is the flow density, $\vec{u}$ the flow speed, $P = \rho T$ the fluid pressure, T the temperature and μ, λ are the shear and bulk dynamic viscosities respectively (for the present case of quasi-incompressible flow with div $\vec{u} \sim 0$ the latter can safely be ignored). Finally, $\vec{u}\vec{u}$ denotes the dyadic tensor $u_a u_b$, $a, b = x, y, z$.

Multispecies transport with chemical reactions is described by a set of generalized continuity-diffusion equations for N_s species:

$$\partial_t C_s + \text{div } C_s \vec{u} = \text{div}[D_s C_T \nabla(C_s/C_T)] + \dot{\Omega}_s \delta(\vec{x} - \vec{x}_w)$$
$$s = 1, N_s \tag{3}$$

where C_s denotes the mass density of the generic sth species, D_s its mass diffusivity, $C_T = \sum_s C_s$ the total mass of transported species and $\dot{\Omega}_s$ is a chemical reaction term which is non-zero along the reactive surface described by the coordinate $\vec{x}_w$. Note that the diffusive term on the right-hand-side of Eq. (3) secures mass conservation upon summation over all species because $C_T = \sum_s C_s$ (we assume $D_s = D$ for all species).

According to Fick's law, the outgoing (bulk-to-wall) diffusive mass flow is given by:

$$\Gamma_w = \int_S u_\perp C|_{\text{wall}} - D\partial_\perp C|_{\text{wall}} \, dS \tag{4}$$

where $\perp$ denotes the normal-to-wall coordinate and S is the area of the exchange surface between the fluid and the solid wall. Upon contact with solid walls, the transported species react according to the following empirical rate equation (the species index being removed for simplicity):

$$\dot{\Omega} \equiv \frac{dC^w}{dt} = \frac{\Gamma_w}{V} - K_c C^w \tag{5}$$

where V is the reaction volume. The wall-flux is taken in the simple linear form:

$$\Gamma_w = K_w(C^g - C^w)\, V \tag{6}$$

where K_w is the wall to/from fluid mass transfer rate and K_c is the chemical reaction rate dictating species consumption once a molecule is absorbed by the wall. The subscripts w and g mean "wall" (solid) and "gas" in a contact with the wall respectively. The above rate equation serves as a dynamic boundary condition for the species transport equations, so that each boundary cell can be regarded as a microscopic chemical reactor sustained by the mass inflow from the fluid. In the absence of surface chemical reactions the species concentration in the solid wall would pile up in time, up to the point where no outflow would occur, a condition met when $C^g = C^w$. Chemistry sets a time scale for this pile-up and fixes the steady-state mass exchange rate. At steady state we obtain:

$$C^w = \frac{K_w}{K_w + K_c}\, C^g \tag{7}$$

hence

$$\Gamma^w = \frac{C^g}{\tau_w + \tau_c} \tag{8}$$

where $\tau_w = 1/K_w$ and $\tau_c = 1/K_c$. These expressions show that finite-rate chemistry ($K_c > 0$) ensures a non-zero steady wall outflux of pollutant. At steady state, this mass flow to the catalytic wall comes into balance with chemical reactions, thus fixing a relation between the value of the wall concentration and its normal-to-wall gradient (we set $\vec{u}_\perp|_w = 0$):

$$-D\partial_z C^g|_w = \delta\, C_g / (\tau_c + \tau_w)$$

where δ is the thickness (volume/area) of the reactive cell. This is a mixed Neumann-Dirichlet boundary condition which identifies the free-slip length of the tracer as:

$$l_s = D(\tau_w + \tau_c)/\delta$$

This expression shows that in the limit of infinitely fast chemistry and wall transfer, the free-slip length tends to zero so that the cross-flow distribution of the tracer develops a vanishingly thin near-wall boundary layer ("reaction sheet"). In actual practice, the fluid cells in contact with reactive boundary cells receive a diffusive-advective mass flux from the bulk flow [Eq. (4)] and transfer to the wall a contribution given by Eq. (6).

3. THE COMPUTATIONAL METHOD

The flow field is solved by a lattice Boltzmann method[4–7] while the multi-species transport and chemical reactions are handled with a variant of the Lax–Wendroff method.[8] A few details are given in the following.

3.1. Lattice Boltzmann Equation

The simplest, and most popular form of lattice Boltzmann equation (Lattice BGK, for Bhatnagar, Gross, Krook),[7] reads as follows:

$$f_i(\vec{x}+\vec{c}_i, t+1) - f_i(\vec{x}, t) = -\omega[f_i - f_i^e](\vec{x}, t) \tag{9}$$

where $f_i(\vec{x}, t) \equiv f(\vec{x}, \vec{v}=\vec{c}_i, t)$ is a discrete distribution function moving along the discrete speed $\vec{c}_i$. The set of discrete speeds must be chosen in such a way as to guarantee mass, momentum and energy conservation, as well as rotational invariance. Only a limited subclass of lattices qualifies. In the sequel, we shall refer to the nineteen-speed lattice consisting of zero-speed, speed one $c = 1$ (nearest neighbor connection), and speed $c = \sqrt{2}$, (next-nearest-neighbor connection). This makes a total of 19 discrete speeds, 6 neighbors, 12 nearest-neighbors and 1 rest particle ($c = 0$). The right hand side of (9) represents the relaxation to a local equilibrium f_i^e in a time lapse of the order of ω^{-1}. This local equilibrium is usually taken in the form of a quadratic expansion of a local Maxwellian:

$$f_i^e = \rho w_i \left[1 + \frac{\vec{u} \cdot \vec{c}_i}{c_s^2} + \frac{\vec{u}\vec{u} \cdot (\vec{c}_i\vec{c}_i - c_s^2 I)}{2c_s^4} \right] \tag{10}$$

where w_i is a set of weights, $w_i = 4/9, 1/9, 1/36$ for particles of speed $c = 0, 1, \sqrt{2}$ respectively in the 19-speed lattice considered here. Finally, c_s is the lattice sound speed defined by the relation

$$c_s^2 I = \frac{\sum_i w_i \vec{c}_i \vec{c}_i}{d} \tag{11}$$

where d is the space dimensionality and I denotes the identity tensor. For the 19-speed lattice considered here $c_s^2 = 1/3$. The fluid density and speed are obtained by (weighted) sums over the set of discrete speeds:

$$\rho = \sum_i f_i, \qquad \rho\vec{u} = \sum_i f_i \vec{c}_i \tag{12}$$

where we have assumed a unit mass for the fluid particles.

LBE was historically derived as the one-body kinetic equation resulting from many-body Lattice Gas Automata via the following conceptual steps are:

- Neglect of many-body correlations
- Small Knudsen number expansion around _local_ equilibria
- Small Mach number expansion around _global_ uniform equilibria

We remind here that the Knudsen number is the ratio of particle mean-free path versus the smallest hydrodynamic length, whereas the Mach number is the ratio of fluid to sound speed. This analysis shows that the LBE fluid behaves like a quasi-incompressible fluid with kinematic viscosity:

$$v = c_s^2(1/\omega - 1/2)$$

Owing to its flexibility toward grossly irregular geometries, the LBE has proved a very competitive tool for the numerical studies of hydrodynamic flows in grossly irregular geometries since its earliest days.[9]

3.2. Modified Lax–Wendroff Scheme for Species Transport

Numerical schemes to integrate passive/active scalar equations within the LBE formalism come in a variety of choices. The simplest formulations are based on the introduction of an additional set of discrete populations, which evolve according to a simple LBE such that the population density corresponds to the desired scalar concentration C. These schemes are seamlessly coupled to LBE for the fluid flow, but very expensive in computer storage since any additional species requires at least $2d$ discrete populations in spatial dimension d. The other extreme is to couple LB to any generic finite-difference/volume/element solver. This does not waste any computer storage, but may require some interfacing effort with LBE if the finite-difference grid does not coincide with the LBE lattice. A convenient choice in this respect is provided by a variant of the Lax–Wendroff scheme recently developed precisely to address multicomponent fluid transport (and reaction) within a LBE-like language. Here we present a summary of the basic ideas behind this LBE-Lax Wendroff scheme, directing the reader fond of full details to the original reference.[8] The first observation is that since species transport equation is linear in the species concentration, we can solve it on a simple $2d$-neighbors cubic lattice. Within this approach, each species is associated with a species density C_s, which splits into $2d+1$ separate contributions along the lattice links plus

the lattice site itself. To the purpose of a compact notation, it proves expedient to denote the neighborhood of a given node by two indices $l = -1$, 0, 1 and $a = x, y, z$, so that $\vec{x}_{la} = \vec{x} + l\hat{a}$ denotes the neighbor along the direction $\pm a$, $l = 0$ characterizing the node itself.

Note that the transport lattice is simply the subset of the LBE lattice restricted to zero-speed and speed-one particles.

Prior to discretization, a few analytic manipulations of the transport equation are in order. In particular, we recast (3) in the following standard advection-diffusion form

$$\partial_t C_s + \mathrm{div}\, C_s \vec{u}'_s = D_s \Delta C_s \tag{13}$$

where the effective speed $\vec{u}'_s$ is the sum of the fluid speed and an ''apparent'' speed due to inhomogeneities of the total concentration:

$$\vec{u}'_s = \vec{u} + \vec{u}_s \tag{14}$$

$$\vec{u}_s = D_s \frac{\nabla C_T}{C_T} \tag{15}$$

A simple Lax-scheme for Eq. (13) is known to introduce a high numerical viscosity, $D_{\mathrm{num},a} = \frac{1}{2d}(1 - du'^2_a)$ in lattice units. To remove this undesirable effect we add a counter-diffusive term $-D_{\mathrm{num}}\Delta$ to the transport equation, whose consequences shall be commented shortly. After all these preparations, we can finally write the transport operator in d dimensions in full splendor (still lattice units and with species index suppressed for simplicity):

$$C(\vec{x}, t) = \sum_l \sum_a p_{la}(t-1)\, C(\vec{x}_{la}, t-1) + q_{la}(t-1) \tag{16}$$

where:

$$p_{la}(t-1) = \frac{1}{2}\left(\frac{1}{d} + lu'_a\right) + D'_a, \qquad l = \pm 1 \tag{17}$$

$$D'_a = D - \frac{1}{2d}(1 - du'^2_a) \tag{18}$$

$$p_0 = -2\sum_a D'_a \tag{19}$$

$$q_{la}(t-1) = -\frac{l}{8} u'_a \sum_{b \neq a} u'_b \sum_l l\, C(\vec{x}_{la}) \tag{20}$$

with u'_a is evaluated at $\vec{x}_{la}$, $t-1$. The transition coefficients p_{la} represent the contribution to the concentration at $\vec{x}$ at time t from the neighbor $\vec{x}_{la}$ at $t-1$. The sources q_{la} collect instead the contribution of the next-to-nearest neighbors, which are due exclusively to second order cross-derivatives of the velocity-dependent component of the effective diffusivity D'_a. It is readily checked that transition probabilities and sources obey the following sum rules:

$$\sum_{la} p_{la} = 1 \tag{21}$$

$$\sum_{la} q_{la} = 0 \tag{22}$$

This rearrangement proves fairly convenient from both computational and analytical purposes. In fact, it can be be shown by linear stability analysis that the resulting Lax–Wendroff scheme becomes *hyper-diffusive* (diffusion effects are shifted to *fourth-order*) without loosing stability (see Appendix of ref. 8). This is a very useful property for reactive flow simulations. The same analysis, as well as numerical experiments, also show that the scheme is affected by phase-errors which tend to develop spurious wiggles (Gibbs phenomena) if the fluid moves ''too fast,'' meaning by this a cell-Péclet number in excess of about ten: $\frac{u'}{D} > 10$ in lattice units. This qualifies the present Lax–Wendroff scheme as a good candidate for (relatively) slow reactive flows, such as those addressed in the present work.

3.3. Multiple Time Scales

The simulation of a reactive flow system is to all effects a *multi-physics* problem involving five distinct time scales:

1. *Fluid Advection and Diffusion*

$$\tau_A = L/U,$$
$$\tau_v = H^2/v \tag{23}$$

where L, H are the length and height of the fluid domain.

2. *Species Diffusion, Wall-Mass Transfer and Reaction*

$$\tau_D = H^2/D,$$
$$\tau_w = K_w^{-1}, \tag{24}$$
$$\tau_c = K_c^{-1}$$

As discussed in the introduction, these time scales define the major dimensionless parameters

$$\mathrm{Re} = UH/v \equiv \tau_A/\tau_v, \tag{25}$$

$$\mathrm{Pe} = UH/D \equiv \tau_D/\tau_A, \tag{26}$$

$$\mathrm{Da}_c = \tau_f/\tau_c, \qquad \mathrm{Da}_w = \tau_f/\tau_w \tag{27}$$

where f stands for fluid advection and/or diffusion.

To acknowledge the simultaneous presence of multiple time scales, a sub-cycled time-stepper is adopted. This is organized as follows. The code ticks with the hopping time of the fluid populations from a lattice site to its neighbors $dt = 1$. Under all circumstances dt is much smaller than both diffusive and advective fluid scales in order to provide a faithful description of fluid flow and transport. Whenever dt exceeds the chemical/wall transfer time-scales, *fractional time-stepping*, i.e., sub-cycling of the corresponding process is performed. This means that the chemical and wall transfer operators are performed dt/τ_c, dt/τ_w times respectively at each fluid cycle. As it will be appreciated shortly, since the flow solver ticks at the sound speed, the present microflow simulations proceed in very short time steps, of the order of tens of nanoseconds. This means that the present scheme can in principle be coupled to mesoscopic methods, such as kinetic Monte Carlo, affording a more fundamental description of the fluid-wall interactions.

4. CATALYTIC EFFICIENCY: QUALITATIVE ANALYSIS

Ideally, we would like to synthesize a universal functional dependence of the catalytic efficiency as a function of the relevant dimensionless numbers and geometrical design parameters:

$$\eta = F(\mathrm{Re}, \mathrm{Da}, \mathrm{Pe}; \bar{g}) \tag{28}$$

where $\bar{g}$ represents a vector of geometric parameters characterizing the boundary shape. The question is to assess the sensitivity of η to $\bar{g}$ and possibly find an optimal solution (maximum η) within the given parameter space. Mathematically, this is a complex non-linear functional optimization problem.[10] We find it convenient to start from a simple—and yet representative—baseline geometry as an "unperturbed" zeroth order approximation, which is easily accessible either analytically or numerically. Perturbations to this baseline situation can then be parametrized as "topological excitations" on top of the geometrical "ground state." In the present study, the unperturbed geometry is a straight channel of size L along the flow direction (x)

and $H \times H$ across it (y, z). Perturbations are then defined as micro-corrugations in the bottom wall of the form $z = h(x, y)$, $h \equiv 0$ being the smooth-wall unperturbed case. An important design parameter is the device efficiency, defined as the amount of pollutant burned per unit mass injected:

$$\eta = \frac{\Phi_{\text{in}} - \Phi_{\text{out}}}{\Phi_{\text{in}}} \qquad (29)$$

where

$$\Phi(x) = \int [uC](x, y, z) \, dy \, dz \qquad (30)$$

is the longitudinal mass flow of the pollutant at section x. The in-out longitudinal flow deficit is of course equal to the amount of pollutant absorbed at the catalytic wall, namely the normal-to-wall mass flow rate:

$$\Gamma = \int_S \vec{\gamma}(x, y, z) \cdot d\vec{S} \qquad (31)$$

where the flux consists of both advective and diffusive components:

$$\vec{\gamma} = \vec{u}C - D\nabla C \qquad (32)$$

and the integral runs over the entire absorbing surface S. The goal of the optimization problem is to maximize Γ at a given Φ_{in} and S, or, conversely, minimize S at a given Φ_{in}. As it is apparent from the above expressions, this means maximizing complex configuration-dependent quantities, such as the wall distribution of the pollutant and its normal-to-wall gradient. For future purposes, we find it convenient to recast the catalytic efficiency as $\eta = 1 - T$, where T is the channel *transmittance*, defined as:

$$T \equiv \Phi_{\text{out}} / \Phi_{\text{in}} \qquad (33)$$

basically the probability for a tracer molecule injected at the inlet to exit the channel without being absorbed by the wall. Roughly speaking, this is controlled by the ratio of advection to diffusion time scales. More precisely, the escape rate is high if the cross-channel distance walked by a tracer molecule in a transit time τ_A is much smaller than the channel cross-length $H/2$. Mathematically: $D\tau_A \ll H^2/4$, which is:

$$\text{Pe} \gg 4L/H \qquad (34)$$

The above inequality (in reverse) shows that in order to achieve high conversion efficiencies, the longitudinal aspect ratio L/H of the device has to scale linearly with the Péclet number.

4.1. Efficiency of a Smooth Channel: Analytic and Scaling Considerations

For a smooth channel, the steady state solution of the longitudinal concentration field away from the inlet boundary factors into the product of three independent one-dimensional functions: $C(x, y, z) = X(x) \, Y(y) \, Z(z)$. Replacing this ansatz into the steady-state version of Eq. (3) we obtain:

$$X(x) = X_0 e^{-x/l}$$
$$Y(y) = Y_0 \sin(y/l_y) \tag{35}$$
$$Z(z) = Z_0 \sin(z/l_z)$$

with the longitudinal and cross-flow absorption lengths related via:

$$l = (l_y^2 + l_z^2) \frac{\bar{U}}{D} \tag{36}$$

where $\bar{U}$ is the average flow speed

$$\bar{U}(x) = \sum_{y, z} u(x, y, z) \, C(x, y, z) \Big/ \sum_{y, z} C(x, y, z) \tag{37}$$

Note that because we stipulate that only the top and bottom walls host catalytic reactions, the profile along the span-wise coordinate y remains almost flat, so that we can define a transversal cross-flow diffusion length $l_\perp \sim l_y$. To determine the cross-flow diffusion length $l_\perp$ we impose that along all fluid cells in a contact with the wall, the diffusive flux is exactly equal to fluid-to-wall outflow, namely:

$$\frac{C}{l_\perp^2} = \frac{C_g}{\tau} \frac{2}{N_z} \tag{38}$$

where τ the effective absorption/reaction time scale,

$$\frac{1}{\tau} \sim \frac{1}{\tau_D} + \frac{1}{(\tau_c + \tau_w)} \tag{39}$$

and the factor $2/N_z$ is the fraction of reactive cells along any given cross-section $x = $ const. of the channel. The form factor C_g/C is readily obtained by the third of Eqs. (35) which yields

$$\frac{C_g}{C} \simeq \cos(H/2l_\perp) \tag{40}$$

Combining this equation with Eq. (38) we obtain a non-linear algebraic equation for $l_\perp$:

$$\lambda^2 \cos(1/2\lambda) = \frac{D\tau}{H^2}\frac{N_z}{2} \tag{41}$$

where we have set $\lambda \equiv l_\perp/H$. For each set of parameters this equation can be easily solved numerically to deliver $l_\perp$, hence l via the Eq. (36). Given the exponential dependence along the stream-wise coordinate x, the efficiency can then be estimated as:

$$\eta_0 \simeq 1 - e^{-L/l} \tag{42}$$

Note that in the low absorption limit $L \ll l$, the above relation reduces to $\eta_0 \sim L/l$, meaning that halving, say, the absorption length implies same efficiency with a twice shorter catalyzer. In the opposite high-absorption limit, $L \gg l$, the relative pay-off becomes increasingly less significant.

4.2. Efficiency of a Corrugated Channel: Analytical Estimates

Having discussed the baseline geometry, we now turn to the case of a "perturbed" geometry. Let us begin by considering a single barrier of height h on the bottom wall (see Fig. 1). The reference situation is a smooth channel at infinite-Damkohler (infinitely fast chemistry) with $\eta_0 = 1 - e^{-L/l}$. We seek perturbative corrections in the smallness parameter

$$g \equiv h/H$$

representing the the coupling-strength to geometrical perturbations and, more practically, a measure of the relative amount of reactive extra-surface contributed by the corrugation.

The unperturbed wall-flux is

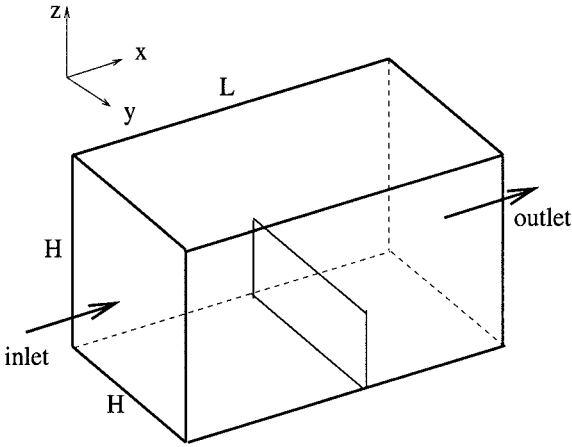$$\Gamma_0 \sim 2D \frac{C_h}{h} LH \tag{43}$$

Fig. 1.   Typical geometrical set up with a single barrier.

where C_h/h is an estimate of the normal-to-wall diffusive gradient. The geometrical gain due to extra-active wall surface is

$$\Gamma_1 \simeq C_h u_h h H \tag{44}$$

where

$$u_h \simeq 4 U_0 (g - g^2) \tag{45}$$

is the average longitudinal flow speed in front of the barrier. The shadowed region of size w in the wake of the obstacle yields an (advective) contribution

$$\Gamma_2 \sim a D \frac{C_h}{h} w H \tag{46}$$

where the coefficient a is a measure of the absorption activity in the wake region.

Three distinctive cases can be identified:

• $a < 1$: The wake absorption is smaller than with unperturbed flow (geometrical shielding prevails)

• $a = 1$: The wake absorption is exactly the same as for unperturbed flow

• $a > 1$: The wake absorption is higher than with unperturbed flow (back-flowing micro-vortices can hit the rear side of the barrier).

Combining these expressions we obtain the following expression:

$$\frac{\delta\eta}{\eta_0} = \frac{\Gamma_1 + \Gamma_2 - \Gamma_2(h=0)}{\Gamma_0} \sim \frac{h}{2L}\,\text{Re}_h(\text{Sc} + K(a-1)) \tag{47}$$

where $\text{Sc} = v/D$ is the Schmidt number (fluid viscosity/tracer mass diffusivity) and the wake length can be estimated as $w = K\,\text{Re}_h$ with $K \sim 0.1$.

The above expression shows a perturbative (quadratic) correction in h over the unperturbed (smooth channel situation). However, since the effective absorption in the shielded region is affected by non-linear phenomena, the factor a may itself exhibit a non-perturbative dependence on h.

5. APPLICATION: FAST-REACTIVE FLOW OVER A MICRO-BARRIER

The previous computational scheme has been applied to a fluid flowing in a millimeter-sized box of size $2 \times 1 \times 1$ millimeters along the x, y, z directions with a single barrier of height h on the bottom wall (see Fig. 1). The fluid flow carries a bulk-passive pollutant, say an exhaust gas flow, which is absorbed at the channel walls where it reacts due to heterogeneus catalysis. The flow is forced with a constant volumetric force which mimics the effects of a pressure gradient. The exhaust gas is continuously injected at the inlet, $x = 0$, with a flat profile across the channel and, upon diffusing across the flow, it reaches solid walls where it gets trapped and subsequently reacts according to a first order catalytic reaction:

$$C + A \rightarrow P \tag{48}$$

where A denotes an active catalyzer and P the reaction products. The initial conditions are:

$$C(x, y, z) = 1, \qquad x = 1 \tag{49}$$

$$C(x, y, z) = 0, \qquad \text{elsewhere} \tag{50}$$

$$\rho(x, y, z) = 1 \tag{51}$$

$$u(x, y, z) = U_0, \qquad v(x, y, z) = w(x, y, z) = 0 \tag{52}$$

The pollutant is continuously injected at the inlet and released at the open outlet, while flow periodicity is imposed at the inlet/outlet boundaries. On the upper and lower walls, the flow speed is forced to vanish, whereas the fluid-wall mass exchange is modeled via a mass transfer rate equation of the form previously discussed. We explore the effects of a sub-millimeter barrier of height h on the bottom wall. The idea is to assess the effects of

the barrier *height*, h on the chemical efficiency. Upon using a $80 \times 40 \times 40$ computational grid, we obtain a lattice with $dx = dy = dz = 0.0025$ (25 microns), and $dt = c_s\, dx/V_s \sim 50 \cdot 10^{-9}$ (50 nanoseconds). Here we have assumed a sound speed $V_s = 300$ m/s and used the fact that the sound speed is $c_s = 1/\sqrt{3}$ in lattice units. Our simulations refer to the following values (in lattice units): $U_0 \sim 0.1 - 0.2$, $D = 0.1$, $v = 0.01$, $K_C = K_W = 0.1$. This corresponds to a diffusion-limited scenario:

$$\tau_c = \tau_w = 10 < \tau_A \sim 800 < \tau_D = 16000 < \tau_v = 160000 \qquad (53)$$

or, in terms of dimensionless numbers:

$$\text{Pe} \sim 40, \quad \text{Re} \sim 400, \quad \text{Da}_A = 80, \quad \text{Da}_D = 1600 \qquad (54)$$

We consider a single barrier of height h placed in the middle of the bottom wall at $x = L/2$, $z = 0$, with: $h/H = 0.05, 0.1, 0.2$. For the sake of comparison, the case of a smooth wall ($h = 0$) is also included. The typical simulation time-span is $t = 32000$ time-steps, namely about 1.6 milliseconds in physical time, corresponding to two mass diffusion times across the channel. The physico-chemical parameters given above are close to catalytic converter operation, apart from the chemical time scales which have been taken according to a fast-chemistry assumption.

With the above parameters we may estimate the reference efficiency for the case of smooth channel flow. With $\bar{U} \sim 0.1$, and $\tau = 20$, we obtain $l \sim 200$, hence $\eta_0 \sim 0.33$. A typical two-dimensional cut of the flow pattern and pollutant spatial distribution in the section $y = H/2$ is shown in Figs. 2 and 3, which refer to the case $h = 8$ ($h/H = 0.1$). An extended (if feeble) recirculation pattern is well visible past the barrier. Also, enhanced concentration gradients in correspondence of the tip of the barrier are recognized from Fig. 3. A more quantitative information is conveyed by Fig. 4, where the integrated concentration of the pollutant:

$$C(x) = \sum_{y,z} C(x, y, z) \qquad (55)$$

is presented for the cases $h = 0, 2, 4, 8$. The main highlight is a substantial reduction of the pollutant concentration with increasing barrier height. This is qualitatively very plausible since the bulk flow is richer in pollutant and consequently the tip of the barrier "eats up" more pollutant than the lower region. In order to gain a semi-quantitative estimate of the chemical efficiency, we measure the pollutant longitudinal mass *flow*:

$$\Phi(x) = \sum_{y,z} [Cu](x, y, z) \qquad (56)$$
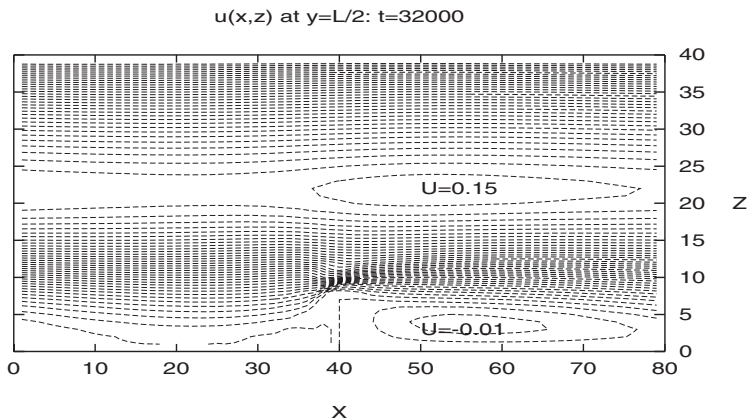
u(x,z) at y=L/2: t=32000

Fig. 2.   Streamwise velocity isocontours with a single barrier of heigth $h = 8$ at $t = 32000$.

The values at $x = 1$ and $x = L$ define the efficiency according to equation (29) (to minimize finite-size effects actual measurements are taken at $x = 2$ and $x = 70$). Leaving aside the initial portion of the channel, our numerical data are well fitted by an exponential with absorption length $l = 200$, in a good agreement with the theoretical estimate $l \simeq 200$ obtained by solving Eqs. (36) and (38). The corresponding results are shown in Table I, where subscript A refers to the analytical expression (47) with $a = 1$.

These results are in a reasonable agreement with the analytical estimate (47) taken at $a = 1$ (same absorption as the smooth channel). However, for $h = 8$ the assumption $a = 1$ overestimates the actual efficiency, indicating
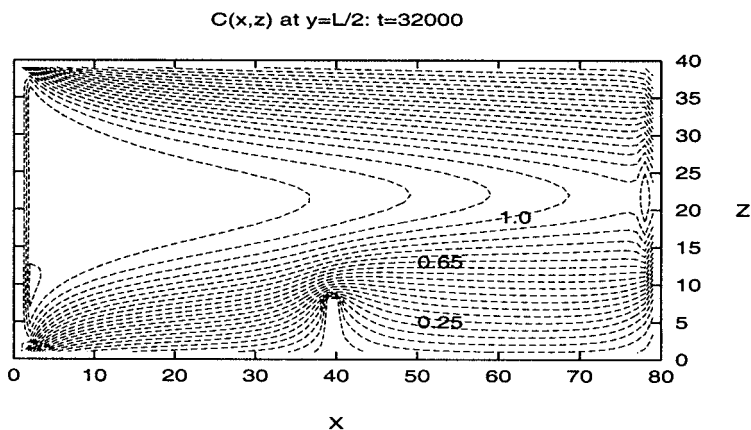
C(x,z) at y=L/2: t=32000

Fig. 3.   Concentration isocontours with a single barrier of heigth $h = 8$ at $t = 32000$.
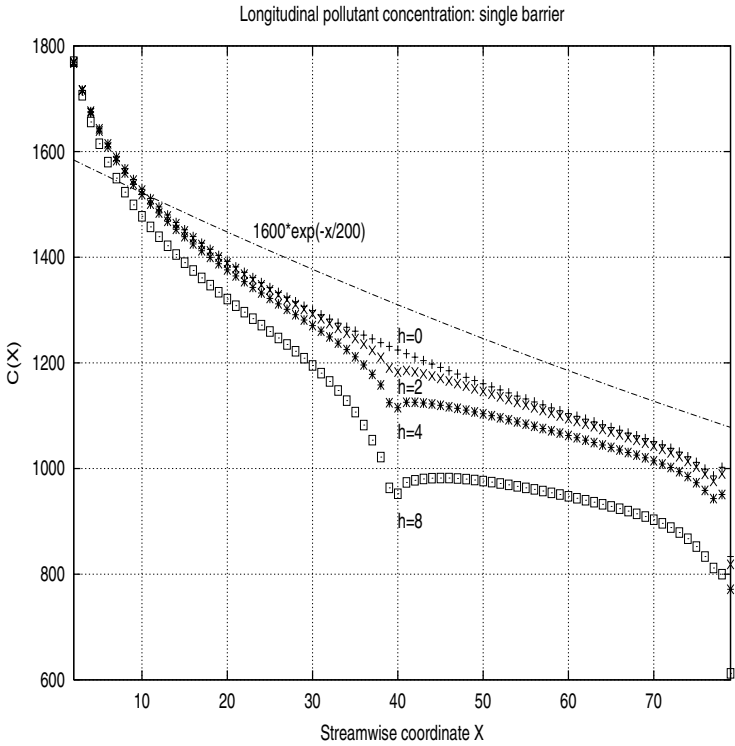
Fig. 4. Integrated concentration $C(x)$ of the pollutant with a single barrier of height $h = 0, 2, 4, 8$ after 32000 steps. The dashed-dotted line represents an exponential fit with the theoretical estimate $l = 200$.

Table I. Single Barrier at $x = 40$: The Effect of Barrier Heigth on the Catalytic Efficiency. Second Column: Barrier Height versus Channel Height. Third Column: Conversion Efficiency, Numerical Data. Fourth Column, Left: Relative Perturbation Due to the Barrier, Numerical Results. Fourth Column, Right: Relative Perturbation Due to the Barrier, Analytical Estimate

Run	h/H	η	$\frac{\delta\eta}{\eta}, \frac{\delta\eta_A}{\eta_A}$
R00	0	0.295	0.00
R02	1/20	0.301	0.02,0.025
R04	1/10	0.312	0.06,0.10
R08	2/10	0.360	0.22,0.40

that the shielded region absorbs less pollutant than in the smooth-channel scenario. Indeed, inspection of the transversal concentration profiles (Fig. 5) along the chord $x = 3L/4$, $y = H/2$ reveals a neat depletion of the pollutant in the wake region due to the shielding effect of the barrier. Besides this efficiency-degrading effect, the barrier also promotes a potentially beneficial flow recirculation, which is well visible in Fig. 6 showing the time evolution of the stream-wise velocity $u(z)$ in the mid-line $x = 3L/4$, $y = H/2$ at $t = 3200$ and $t = 32000$. This figure reveals that recirculating back-flow only sets in for $h = 8$. However, these recirculation effects are feeble (the intensity of the recirculating flow is less than ten percent of the bulk flow) and depletion remains the dominant mechanism. In fact for $h = 8$ the measured local Péclet number is of the order $0.01 \cdot 8/0.01 = 0.8$, seemingly too small to promote appreciable micro-turbulent effects. We conclude that, for blunt obstacles such as perpendicular barriers, shielding effects are likely to outdo the benefits of recirculation. It

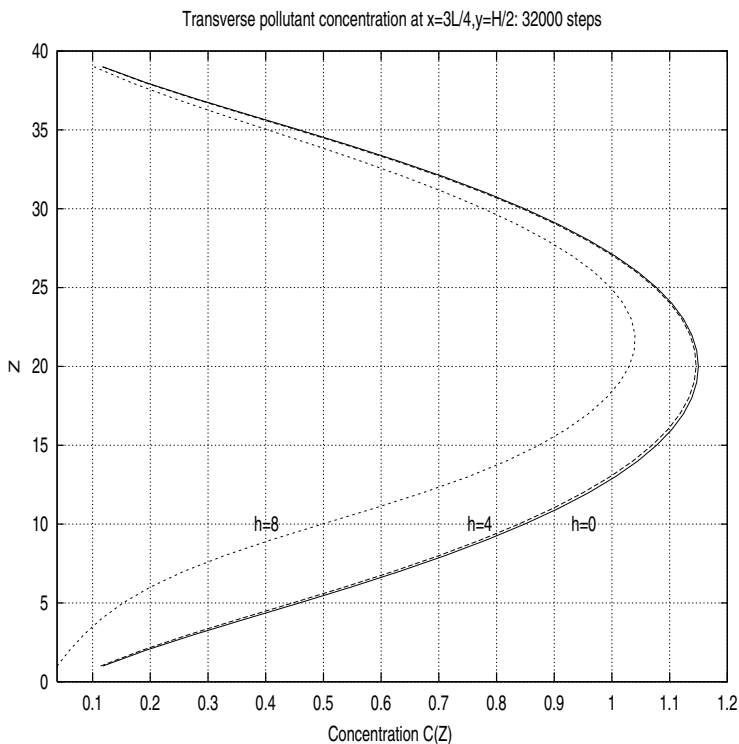Transverse pollutant concentration at x=3L/4,y=H/2: 32000 steps

Fig. 5.   Transverse pollutant concentration $C(z)$ at $x = 3L/4$ and $y = H/2$. Single barrier of varying height, $h = 0, 4, 8$ at $t = 32000$.
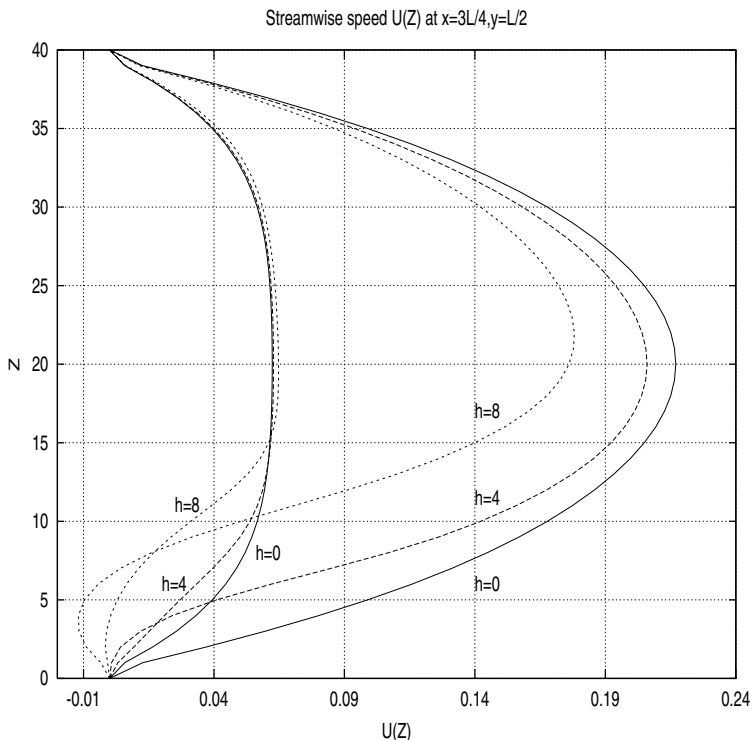
Fig. 6. Time evolution of the transversal streamwise speed $u(z)$ at $x = 3L/4$ and $y = L/2$ at $t = 3200$ and $t = 32000$. Single barrier of varying height $h = 0, 4, 8$. The two curves for each value of h refer to $t = 3200$ and $t = 32000$.

should also be noticed that raising the barrier height has an appreciable impact on the bulk flow as well, which displays some twenty percent reduction due to mechanical losses.

6. TRAPEZOIDAL CORRUGATION

As a second application, we investigate a trapezoidal corrugation, a case of practical relevance for automotive catalytic applications. The reference situation is a fluid flow consisting of an *exhaust gas* at at $P = 1$ Atm and $T = 600°K$, carrying carbon mono-oxide CO as a main pollutant. The exhaust gas is continuously injected at the inlet, $x = 0$, and upon reaching solid walls, carbon mono-oxide reacts with oxygen molecules according to the catalytic reaction:

$$2CO + O_2 = 2CO_2 \tag{57}$$

The initial conditions in the bulk flow are:

$$\rho_{CO} = 0, \qquad \rho_{gas} = \text{const.} \tag{58}$$

$$u_x = \text{const.}, \qquad u_y = u_z = 0 \tag{59}$$

We consider a $3 \times 1 \times 1$ millimeter channel, traversed by a flow at a speed of the order of 10 meters/second. Carbon mono-oxide is continuously injected at the inlet and released at the open outlet. In the present work, we explore the effects of a 0.1 millimeter-high trapezoidal micro-corrugation on the bottom wall with height h and 45° degrees side angles (see Sketch 1). Our simulations refer to the following values (in lattice units): $u \sim 0.1$, $D = 0.1$, $v = 0.01$, $K_C = K_W = 0.001$, corresponding to a slow-chemistry scenario (in lattice units):

$$\tau_A \sim 600, \qquad \tau_C = \tau_W = 1000 < \tau_D = 4000 \tag{60}$$

$$\text{Re} \sim 200, \qquad \text{Pe} \sim 20, \qquad \text{Da}_A \sim 0.6, \qquad \text{Da}_D \sim 4 \tag{61}$$

The physico-chemical parameters given above are close to the working conditions of a catalytic converter, except for the chemical time scale, which, in order to reduce the simulation time-span is placed in the 100 microseconds range, about an order of magnitude faster than ordinary values.

```
        ..............................................
        ..............................................
        ..............................................
    ..... FFFFFFFFFFFFFFFFFFFFFFFFFFFFFFFFFFFFFFFFF .....
    ..... FFFFFFFFFFFFFFFFFFFFFFFFFFFFFFFFFFFFFFFFF .....
    ..... FFFFFFFFFFFFFFFFFBBBBBBBFFFFFFFFFFFFFFFFFF .....
    ..... FFFFFFFFFFFFFFFFFB         BFFFFFFFFFFFFFFFFF .....
    ..... FFFFFFFFFFFFFFFFB           BFFFFFFFFFFFFFFFF .....
    ..... FFFFFFFFFFFFFFFB             BFFFFFFFFFFFFFFF .....
    ..... BBBBBBBBBBBBBBB             BBBBBBBBBBBBBB .....
```

Sketch 1.   Template of a trapezoidal corrugation with $h = 4$ in a x–z cross section. Each letter represents a lattice site. F: fluid, B: boundary. (The vertical direction is stretched out.)
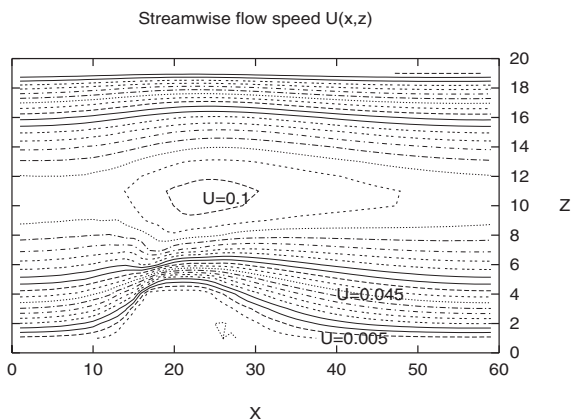
Streamwise flow speed U(x,z)

Fig. 7.   Streamwise velocity field in the mid-span cross-section, $y = 10$ at $t = 12000$.

Let us now come to the actual results. A typical two-dimensional cut of the flow pattern is shown in Fig. 7, from which a high-shear flow in the near-obstacle region is again apparent. The corresponding two-dimensional CO pattern is shown in Fig. 8. The integrated concentration along the channel is shown in Fig. 9. Much of the observed depletion is purely geometrical (the channel restriction) and the truly dynamical effect is best appreciated by inspecting the longitudinal longitudinal outflow $\Phi(x)$. Comparison with the smooth-channel scenario shows a very tiny but yet visible effect (see Fig. 10). Inspection of the actual numbers (taken 20 sites away from the outlet in order to minimize boundary effects) yield $T_0 = 0.953$ (smooth channel) and $T = 0.946$, namely $\eta_0 = 0.047$ versus
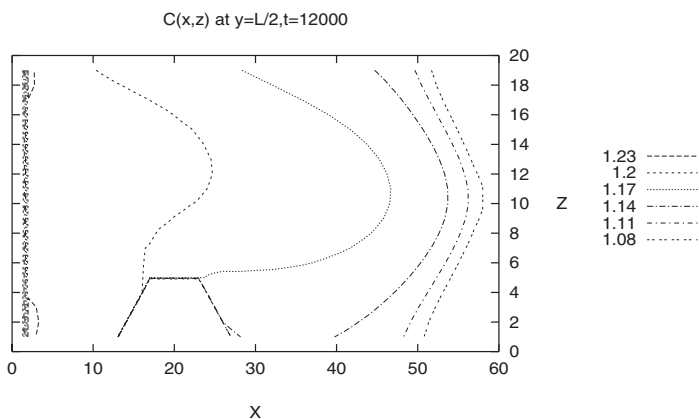
C(x,z) at y=L/2,t=12000

Fig. 8.   Isocontours of the CO concentration in the mid-span section $y = 10$ at $t = 12000$.
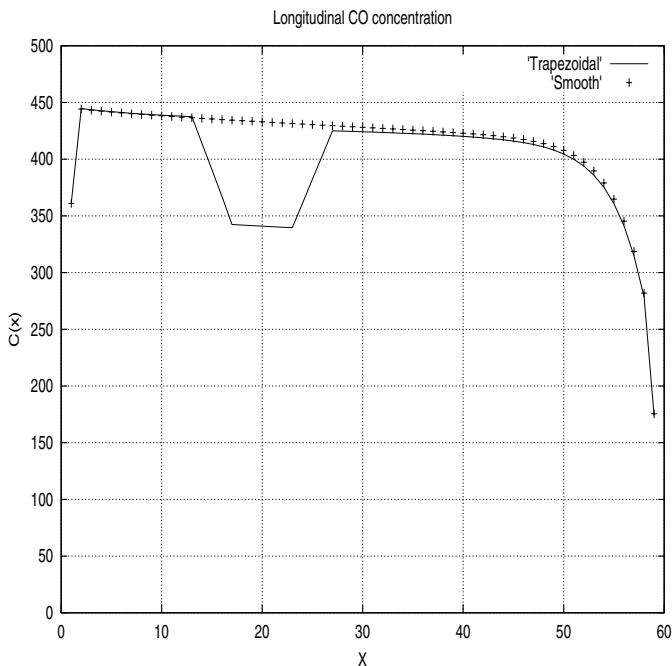
Longitudinal CO concentration

Fig. 9.   Integrated longitudinal CO mass concentration at $t = 12000$. Solid line: corrugated wall, crosses: smooth wall.

$\eta = 0.054$. This corresponds to $\delta\eta/\eta_0 \sim 0.15$, which is significantly higher than the purely geometrical increase of the reactive surface:

$$2h(\sqrt{2}-1)/2L \sim 0.053$$

This is not surprising since owing to the relatively smooth shape of the obstacle, the flow "sticks" closely to the trapezoidal corrugation with only a minor detachment in the wake region, so that it can benefit of enhanced cross-flow concentration gradients. The conclusion is that relatively smooth obstacles are likely to provide a better catalytic efficiency.

6.1. Up-Scaling to Macroscopic Devices

It is important to realize that even tiny improvements on the microscopic scale can result in pretty sizeable cumulative effects on the macroscopic scale of real devices, say 10 centimeters in the case of catalytic converters. Let us
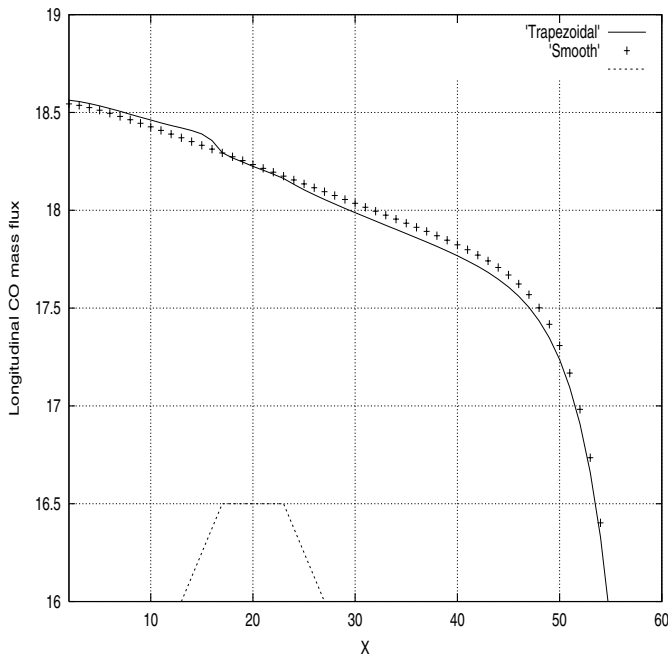
Fig. 10.   Longitudinal CO mass flow rate at $t = 12000$.

assume for simplicity that the efficiency of an array of N serial micro-channels can be estimated simply as

$$\eta_N = 1 - T^N \tag{62}$$

On a scale of $L = 10$ centimeters ($N = 50$) our simulation yields $\eta_0 = 0.973$ and $\eta = 0.984$, much higher than experimental observation. This is due to the artificially faster chemistry used to save computing time. Realistic (and time consuming) simulations with ten times slower chemistry yield $R_0 = 0.977$, $R = 0.972$, which on a scale of 10 centimeters, correspond to $\eta_0 \sim 0.687$ and $\eta \sim 0.758$, in a good agreement with experimental evidence and previous two-dimensional simulation work.[11] It is clear that extrapolation to macroscopic scales based on the equation (62) must be taken very cautiously. In fact, a tight synergy between computer simulation and analytical scaling theories is called for in order to make robust predictions at the macroscopic scale.

7. CONCLUSIONS

This work presents an exploratory study of the complex hydro-chemical phenomena which control the effective reactivity of catalytic devices of millimetric and centimetric size. These simulations shed light on the competition between various non-perturbative effects, such as shielding and micro-recirculation in the wake of geometrical obstrusions, which are hardly amenable to analytical treatment. It is hoped that the flexibility of the present computer tool, as combined with semi-analytical scaling theories, can be of significant help in developing semi-quantitative intuition about the subtle and fascinating interplay between geometry, chemistry, diffusion and hydrodynamics in the design of chemical traps, catalytic converters and other related devices.[12]

ACKNOWLEDGMENTS

REFERENCES

1. F. Abraham, J. Broughton, N. Bernstein, and E. Kaxiras, *Comp. in Phys.* **12**:538 (1998).
2. E. Oran and J. Boris, *Numerical Simulation of Reactive Flows* (Elsevier Science, New York, 1987).
3. G. Ertl and H. J. Freund, Catalysis and surface science, *Phys. Today* **52**:32 (1999).
4. G. Mc Namara and G. Zanetti, *Phys. Rev. Lett.* **61**:2332 (1988).
5. F. Higuera, S. Succi, and R. Benzi, *Europhys. Lett.* **9**:345 (1989).
6. R. Benzi, S. Succi, and M. Vergassola, *Phys. Rep.* **222**:145 (1992).
7. Y. Qian, D. d'Humieres, and P. Lallemand, *Europhys. Lett.* **17**:149 (1989).
8. S. Succi, G. Bella, A. De Maio, H. Chen, K. Molvig, and C. Teixeira, *J. Comp. Phys.* **152**:493 (1999).
9. A. Cancelliere, E. Chang, E. Foti, D. Rothman, and S. Succi, *Phys. Fluids Lett.* **2**:2085 (1990).
10. F. Stepanek, M. Kubicek, M. Marek, and P. Adler, *Chem. Eng. Sci.* **54**:1493 (1999).
11. A. Bergmann, R. Bruck, and C. Kruse, Society of Automotive Engineers (SAE) technical paper SAE 971027, Proceedings of the 1997 International SAE Congress, Detroit, USA, February 1997.
12. S. Succi, O. Filippova, G. Smith, and E. Kaxiras, *Comput. Sci. Eng.* **3**(6):26 (2001).